



## City Research Online

### City, University of London Institutional Repository

---

**Citation:** Moghaddam, E.R., Long, C. & Sayma, A. I. (2013). A numerical investigation of moment coefficient and flow structure in a rotor-stator cavity with rotor-mounted bolts. PROCEEDINGS OF THE INSTITUTION OF MECHANICAL ENGINEERS PART A- JOURNAL OF POWER AND ENERGY, 227(3), pp. 306-327. doi: 10.1177/0957650912473543

This is the draft version of the paper.

This version of the publication may differ from the final published version.

---

**Permanent repository link:** <https://openaccess.city.ac.uk/id/eprint/7106/>

**Link to published version:** <https://doi.org/10.1177/0957650912473543>

**Copyright:** City Research Online aims to make research outputs of City, University of London available to a wider audience. Copyright and Moral Rights remain with the author(s) and/or copyright holders. URLs from City Research Online may be freely distributed and linked to.

**Reuse:** Copies of full items can be used for personal research or study, educational, or not-for-profit purposes without prior permission or charge. Provided that the authors, title and full bibliographic details are credited, a hyperlink and/or URL is given for the original metadata page and the content is not changed in any way.

---

City Research Online:

<http://openaccess.city.ac.uk/>

[publications@city.ac.uk](mailto:publications@city.ac.uk)

---

# Proceedings of the Institution of Mechanical Engineers, Part A, Journal of Power and Energy

## A NUMERICAL INVESTIGATION OF MOMENT COEFFICIENT AND FLOW STRUCTURE IN A ROTOR-STATOR CAVITY WITH ROTOR MOUNTED BOLTS

--Manuscript Draft--

<b>Manuscript Number:</b>	JPE1551
<b>Full Title:</b>	A NUMERICAL INVESTIGATION OF MOMENT COEFFICIENT AND FLOW STRUCTURE IN A ROTOR-STATOR CAVITY WITH ROTOR MOUNTED BOLTS
<b>Article Type:</b>	Original Article
<b>Keywords:</b>	rotating cavities, bolt windage, rotor stator cavity, moment coefficient
<b>Corresponding Author:</b>	Abdulnaser Sayma, PhD University of Sussex Falmer, Brighton, West Sussex UNITED KINGDOM
<b>Corresponding Author Secondary Information:</b>	
<b>Corresponding Author's Institution:</b>	University of Sussex
<b>Corresponding Author's Secondary Institution:</b>	
<b>First Author:</b>	Elham Roshani Moghaddam, PhD student
<b>First Author Secondary Information:</b>	
<b>Order of Authors:</b>	Elham Roshani Moghaddam, PhD student Christopher Long, PhD Abdulnaser Sayma, PhD
<b>Order of Authors Secondary Information:</b>	
<b>Abstract:</b>	<p>ABSTRACT</p> <p>The torque associated with overcoming the losses on a rotating disc is of particular importance to the designers of gas turbine engines. Not only does this represent a reduction in useful work, but it also gives rise to unwanted heating of metal surfaces and the adjacent fluid.</p> <p>This paper presents a numerical study on the effect of rotor-mounted bolts on the moment coefficient and velocity distributions within a rotor-stator cavity under conditions representative of modern gas turbine engine design. Steady-state, 2D and 3D, CFD simulations are obtained using the FLUENT commercial code with a standard k- turbulence model. The model is validated against experimental data and then used to investigate the effects of varying the number of bolts and also a continuous ring. Two test cases are investigated: one corresponds to where the flow structure is dominated by the superimposed flow (<math>T = 0.35</math>); the other, where rotation is expected to govern the flow structure (<math>T = 0.35</math>).</p> <p>It is possible to separate out the contributions due to skin friction and pressure related (form drag and pumping loss) in the CFD results. This shows that the contribution of skin friction to the overall moment coefficient reduces as the number of bolts increases and the pressure related losses increase. There also appears to be a point where increasing the number of bolts does not bring about an increase in the overall moment coefficient. It is also interesting to report that the moment coefficient associated with a continuous ring is similar to that for a plain disc.</p>

# **A NUMERICAL INVESTIGATION OF MOMENT COEFFICIENT AND FLOW STRUCTURE IN A ROTOR-STATOR CAVITY WITH ROTOR MOUNTED BOLTS**

**Elham Roshani Moghaddam, Christopher Long and Abdalnaser Sayma**

Thermo-Fluid Mechanics Research Centre  
**University of Sussex, Brighton, BN1 9QT, U.K.**

## **ABSTRACT**

The torque associated with overcoming the losses on a rotating disc is of particular importance to the designers of gas turbine engines. Not only does this represent a reduction in useful work, but it also gives rise to unwanted heating of metal surfaces and the adjacent fluid.

This paper presents a numerical study on the effect of rotor-mounted bolts on the moment coefficient and velocity distributions within a rotor-stator cavity under conditions representative of modern gas turbine engine design. Steady-state, 2D and 3D, CFD simulations are obtained using the FLUENT commercial code with a standard k- $\epsilon$  turbulence model. The model is validated against experimental data and then used to investigate the effects of varying the number of bolts and also a continuous ring. Two test cases are investigated: one corresponds to where the flow structure is dominated by the superimposed flow ( $\lambda_T = 0.35$ ); the other, where rotation is expected to govern the flow structure ( $\lambda_T = 0.35$ ).

It is possible to separate out the contributions due to skin friction and pressure related (form drag and pumping loss) in the CFD results. This shows that the contribution of skin friction to the overall moment coefficient reduces as the number of bolts increases and the pressure related losses increase. There also appears to be a

point where increasing the number of bolts does not bring about an increase in the overall moment coefficient. It is also interesting to report that the moment coefficient associated with a continuous ring is similar to that for a plain disc.

## NOMENCLATURE

a, b            Inner and outer radii of the disc, respectively

D               Bolt diameter (measured across-flats)

H               Bolt height

$G = s/b$        Gap ratio

M               Moment or torque

$\dot{m}$                Mass flow rate

N               Number of bolts

p               Pressure

$r_s$                Radius of the shaft

r, z,  $\phi$            Radial, axial and tangential coordinates

s               Axial gap between rotor and stator

$s_c$                Seal clearance

U Mean radial velocity

$V_r, V_\phi$  Radial and tangential velocities in a stationary coordinate system.

$\beta = V_\phi / \omega r$  Core rotation factor

$\beta^*$  Value of  $\beta$  when  $C_w = 0$

$\varepsilon_m$  Constant

$\mu$  Dynamic viscosity

$\rho$  Density

$\omega$  Angular velocity

### Subscripts

b Pertaining to the bolt

### Fluid Dimensionless Groups

$$C_m = \frac{M}{1/2 \rho \omega^2 b^5} \quad \text{Moment coefficient}$$

$$C_w = \frac{\dot{m}}{\mu b} \quad \text{Flow Reynolds number}$$

$$\text{Re}_\phi = \frac{\rho \omega b^2}{\mu} \quad \text{Rotational Reynolds number}$$

$$\lambda_T = \frac{C_w}{\text{Re}_\phi^{0.8}} \quad \text{Turbulent flow parameter}$$

## 1 INTRODUCTION AND REVIEW OF PREVIOUS WORK

Increasing the specific power output of a gas turbine engine, and consequently reducing the size of the power plant requires a higher turbine entry temperature of the main gas flow accompanied by a higher pressure ratio. Turbine entry temperatures in modern civil engines are currently above 1600°C, and components in contact with a flow at such high temperatures will rapidly exceed their creep and fatigue limits leading to catastrophic failure. It is only possible to operate at these elevated temperatures because of the internal air system which uses some of the compressor air to cool the turbine discs, blades and nozzle guide vanes. However, air used for cooling will be heated as a result of viscous dissipation as it flows over both rotating and stationary surfaces. A torque needs to be provided to overcome these irreversible losses and this parasitic phenomenon is referred to as *windage*. Skin friction will be the source of windage for a smooth surface. However, it is not uncommon for protrusions such as bolts to be attached to the rotating and stationary surfaces. In this case, form drag will also contribute to windage. More accurate predictions of windage offer potential for improved design of the internal air system, with associated increases in thrust and efficiency. It is worth noting that there will also be a torque associated with the so-called pumping losses which occur as a result of the work done by a protrusion changing the angular momentum of the fluid. It is important to make the distinction between these and windage because the pumping loss term is isentropic. The sum of the irreversible torque (due to windage) and the reversible torque (due to pumping work) is embodied in the moment coefficient which is defined in Equation (3) below.

Early investigations of frictional losses due to rotating discs were carried out by Daily and Nece (1960) and Bayley and Owen (1969). These identified a number of relevant dimensionless parameters. For a disc of outer radius,  $b$ , rotating at an angular velocity  $\omega$ , in a fluid of density  $\rho$ , and dynamic viscosity  $\mu$ , supplied with a superimposed mass flow rate  $\dot{m}$ , the torque is  $M$ . The rotational Reynolds number  $Re_\phi$ , dimensionless flow rate  $C_w$ , and moment coefficient  $C_m$  are defined as.

$$Re_\phi = \frac{\rho \omega b^2}{\mu} \quad (1)$$

$$C_w = \frac{\dot{m}}{\mu b} \quad (2)$$

$$C_m = \frac{M}{1/2 \rho \omega^2 b^5} \quad (3)$$

For an axial gap between the rotating disc and a stationary casing of  $S$ , the gap ratio  $G$  is defined as:

$$G = \frac{S}{b} \quad (4)$$

The flow structure and dependence of the moment coefficient are determined by the flow regime. For no superimposed flow,  $C_w = 0$ , the regimes identified by Daily and Nece are: 1) small  $G$ , laminar flow; 2) large  $G$ , laminar flow; 3) small  $G$ , turbulent flow, 4) large  $G$ , turbulent flow. The interested reader is referred to either the original work or to Figure 6.1 of Owen and Rogers (1989) for more information. As a rough guide, the flow is turbulent for  $Re_\phi > 10^5$  and for turbulent flow,  $G$  is considered to be large when  $G > 0.04$ .

As noted by Owen and Rogers, the presence of superimposed radial flow complicates the boundaries between these regimes. In particular, a large superimposed flow can cause the flow to be turbulent even when there is no

rotation. For the applications reflected in this paper the flow is expected to be turbulent and for the geometries analysed  $G = 0.1$ . Consequently, the description that follows below applies to a turbulent flow regime with a large axial gap.

For no superimposed flow,  $C_w = 0$ , the flow structure comprises separate boundary layers on the rotor and stator and a central core region where there is only tangential motion with about 40% of disc speed. Flow is pumped up the rotor and moves radially inward down the stator. For the case of a superimposed radial flow ( $C_w > 0$ ), increasing the superimposed flow reduces the tangential velocity of the core. For small amounts of superimposed flow, the flow structure in the cavity is dominated by rotation; conversely for large amounts, the flow structure is dominated by the superimposed flow. Owen and Rogers developed a useful parameter to delineate these two regimes. The turbulent flow parameter  $\lambda_T$  takes its definition from a momentum integral solution of the boundary layer equations using 1/7<sup>th</sup> power law velocity profile (Von Karman, 1921).

$$\lambda_T = \frac{C_w}{\text{Re}_\phi^{0.219}} \quad (5)$$

Owen and Rogers also considered the more general case of a rotating disc in a rotating fluid. This is a good approximation to the flow behavior in an unshrouded rotor stator system where the axial gap between the discs exceeds boundary layer thickness. The flow entrained by the rotor is given by:

$$C_{w,ent} = \varepsilon_m \text{Re}_\phi^{0.8} \quad (6)$$

Where the coefficient  $\varepsilon_m$  depends on the core rotation factor  $\beta$ . For  $\lambda_T < \varepsilon_m$ , the flow structure is dominated by rotation and for  $\lambda_T > \varepsilon_m$ , the throughflow dominates. There is no simple closed form relationship to express  $\varepsilon_m(\beta)$  but using a quadratic fit of the tabulated data by Owen and Rogers gives:

$$C_{w,ent} = (0.2242\beta^2 - 0.441\beta + 0.219) \text{Re}_\phi^{0.8} \quad (7)$$

For  $\beta = 0$  (free disc) this gives the well known result:

$$C_{w,ent} = 0.219 \text{Re}_\phi^{0.8} \quad (8)$$

For  $\beta = 0.42$  which corresponds to a rotor stator system with  $C_w = 0$ :

$$C_{w,ent} = 0.073 \text{Re}_\phi^{0.8} \quad (9)$$

Since  $\beta$  depends on  $\lambda_T$ , the above suggests there is no single value of  $\varepsilon_m$  that can be used to delineate the flow regime. However, for a superimposed radial outflow, a value of  $\lambda_T = 0.219$  represents an upper limit to the value of  $\varepsilon_m$  and consequently an upper limit to a flow that is dominated by rotation effects

The experiments of Dibelius et al. (1984) used a test rig with a rotor disc in an enclosed housing. For rotor mounted bolts, they noted a significant increase in the moment coefficient above that of a plain disc. This occurred for both zero superimposed flow and large values of superimposed flow. Also, they used the radial pressure gradient to derive an axial thrust term in order to demonstrate the effects of protrusions. Comparing the axial thrust values, they noticed that the effect of the protrusions on the flow structure was more pronounced when the flow was dominated by rotational effects.

Zimmerman et al. (1986) measured the effect on shaft torque of various bolt designs. Those considered were: staged (i.e. axially stacked concentric bolts of reducing diameter), cylindrical rotor bolts, partially covered and fully covered (by an annular ring) rotor bolts. It was found that eighteen staged bolts on a disc at a radius ratio of  $r_p/b = 0.75$ , increased the measured torque over the plain disc by a factor of 2.5, with further increases for cylindrical shaped bolts. Partially covered bolts, gave little benefit in reducing the overall torque compared to

the uncovered bolts. However, fully covered bolts, gave a significant reduction in moment coefficient compared with the uncovered bolts and a moment coefficient of approximately 25% above that of a plain disc. The effect of a superimposed flow of  $C_w = 2.6 \times 10^4$  was to increase the moment coefficient by 50% for all the bolt designs investigate. The increase in moment coefficient due to the presence of rotor-mounted protrusions was attributed to the superposition of three elements: form drag, skin friction and pumping losses. They found that for a small number of bolts, form drag dominates the additional moment produced, whereas for a large number of bolts the pumping losses become more important. In addition, the authors also suggest a theoretical limit where increasing the number of bolts will actually cause a decrease in the moment coefficient.

The experiments of Millward and Robinson (1989) measured enthalpy rise in the supplied flow. These were carried out with varying the number of bolts, their diameter, circumferential pitch, and projected cross sectional area. With bolts attached to both the rotor, as well as on the stationary casing. They obtained a correlation of their results for bolts attached to the rotor. They also noted that the effect on enthalpy rise of bolts located towards the outer radius was very significant, whereas those located towards the inner radius had little effect. For stator-mounted bolts, there was insufficient data to derive a correlation, but it was noted that the enthalpy rise due to stator bolts was about one-third of the corresponding conditions with rotor bolts. Tests were also carried out with full and partial covering of both stator and rotor bolts. No measurable effect was found by partially covering the rotor bolts but the stator bolts showed a reduction in enthalpy rise at high mass flows. Fully covered bolts, however, gave similar results to a plain disc and in some cases a reduction was actually observed.

Gartner (1997) developed a semi-empirical correlation that gives satisfactory agreement for the moment coefficient from a plain disc over a wide range of dimensionless mass flows. Gartner (1998) used a momentum integral method to predict the frictional torque from a single disc with protrusions. The predictions agree well

with available data, providing the spacing between the bolts is not so small that wake effects become significant.

Coren (2007) carried out an experimental study on windage effects in rotor-stator cavities. Tests were carried out with bolts mounted on the rotor or on the stator. He suggested correlations for the moment coefficient as a function of the number, size and location of the bolts. Laser Doppler Anemometry (LDA) was also used to measure the radial and tangential components of velocity.

## **2 THE BOLT WINDAGE TEST RIG**

Figure 1 shows a general assembly of the test rig. This consists of a shaft mounted titanium alloy disc of outer radius  $b = 225$  mm enclosed within a sealed steel pressure casing. The maximum clearance between the rotor and casing,  $s = 22$  mm. Around the outer rim of the disc is a labyrinth seal and a stator mounted shroud encases the cavities on either side of the disc. The disc is driven by a 50 kW motor through a 5:1 step up gearbox. Mounted between the gearbox and the disc is an in-line torquemeter. The test side of the disc (labelled ‘front cavity’ in Figure 1) carries the majority of the instrumentation whereas the balance side (labelled ‘rear cavity’) has sufficient instrumentation to balance the flow conditions on both sides of the disc. A superimposed flow of air enters the rig centrally on the test side, flows radially outward through the cavity and leaves through the labyrinth seal at the perimeter. An equal amount of air is supplied to the balance side, where it enters through four inlet pipes equally spaced around the central shaft. There are four orifice plates positioned upstream and downstream of the test rig on both the test and balance side to measure the mass flow of air into and out of the rig and this ensures both sides are balanced. The air is supplied at pressures of up to 7.5 bar (absolute) and mass flows (to both sides) of up to 0.82 kg/s by an Atlas Copco screw type compressor and

treated with an Atlas Copco air conditioning unit to provide dry air in the range 15 to 25 °C prior to delivery to the rig.

A shaft mounted Vibrometer TM112 in line torquemeter measures torque and rotational speed. The 95% confidence interval in torque measurement is less than  $\pm 1$  N m, The uncertainty in speed measurement is less than  $\pm 5$  rev / min. The torque due to bearing friction in the test rig depends on rotational speed and was obtained by a previous calibration. This driveline torque was subtracted from all of the measured values of torque to obtain a value of the torque transmitted to the fluid,  $M$ . The magnitude of the driveline torque varied from approximately 2% of the total at high rotational speeds to approximately 20% at low values of rotational speed.

It is important to note that the test rig was designed with the intention of making the torque on the test and balance sides equal. The two sides have the same geometrical configuration with bolts located on both sides of the disc at the same radius. Furthermore, the pressure was kept equal on both sides of the cavity to provide the same flow conditions. The cooling flow enters into the balance side at a much higher radius ( $r/b = 0.55$ ) than that on the test side ( $r/b = 0.1$ ). As a result the flow travels over a smaller section of disc before exiting the system. There are two reasons why this difference in inlet radius is thought to have an insignificant effect on the torque. Firstly, the torque on a plain disc is a strong function of radius (von Kármán,  $M \propto r^{4.6}$ ). Consequently, most of the contribution to the torque experienced by the balance side comes from that radially outward of the inlet. Secondly, the tangential velocity of the disc at this higher radius will also be proportionally higher, leading to greater shear between the disc and non rotating fluid near the entry point. This will increase the local moment coefficient in this region which will act to balance the torque experienced on each side of the disc.

Tests were carried out with  $N = 3, 9$  and  $18$  and  $D = 16$  mm, hexagonal bolts of height,  $H = 11$  mm. These were attached, at a radius of  $0.2$  m,  $r_b/b = 0.889$ , to both sides of the disc surface to ensure similar conditions on either side and minimizing axial heat conduction. For reference, the orientation of the bolts relative to the direction of rotation is shown in Figure 2.

### 3 VALIDATION OF THE COMPUTATIONAL MODEL

Validation was performed against the plain disc experimental measurements of Coren (2007) carried out on the rotor-stator test rig described in Section 2.

No bolts were attached to either the rotor or stator. The computations were carried out for two cases of interest: 1) throughflow dominated ( $\lambda_T = 0.21$ ,  $C_w = 0.3 \times 10^5$ ,  $Re_\phi = 0.271 \times 10^7$ ); and 2) rotationally dominated ( $\lambda_T = 0.09$ ,  $C_w = 0.3 \times 10^5$ ,  $Re_\phi = 0.81 \times 10^7$ ). The absolute inlet air pressure and temperature for the throughflow dominated case are  $2.04$  bar, and  $294$  K, while for the rotationally dominated one, they are  $3$  bar, and  $301$  K.

A schematic diagram of the geometry modeled is shown in Figure 3. Models of the geometry in two dimensions were built and meshed separately for use with enhanced wall and standard wall treatments. There is an extended geometry after the outlet which is used to avoid reversed flow through the outflow boundary. This extended geometry provides a uniform flow before the outlet boundary, and prevents it from changing direction and re-entry through the outlet, which could cause numerical instability. A grid independence study was carried out in order to make sure that the computational results were unaffected by grid size. To achieve this, the number of grid cells was doubled. Results were then compared with the coarser mesh. If no discrepancies between the two results were considered to be negligible, the coarser mesh was selected for further simulations. The number of points for the grid independent simulation in this case is  $18,000$  with  $200 \times 60$  points in the  $r$ - $z$  plane for use

with the enhanced wall treatment and 9,000 (200 x 30 points in the r-z plane) for use with the standard wall treatment. The segregated, implicit solver was used with the 2<sup>nd</sup> order discretisation method. Results were obtained using a number of different turbulence models so as to determine which provides the best match to the experimental data.

The air is taken to be compressible with the ideal gas law for modeling density and Sutherland's law (three coefficient method) for modeling viscosity. The pressure and temperature boundary conditions used at the inlet for each case were obtained from the experimental data. The outlet pressure was set so that it produced the measured quantity of mass flow rate. A moving reference frame with an angular velocity of the rotor speed was used.

The convergence criteria were as follows:

1. Iterations residual for all the variables form a constant horizontal line and are less than  $10^{-4}$ .
2. The fluctuations of outlet mass flow rate are less than 0.1% of inlet mass flow rate.
3. All computed variables did not change significantly for at least 1000 iterations.

Figure 4 and 5 compare the simulation results of, respectively, the dimensionless radial and tangential velocities at  $r/b = 0.79$  for the rotationally dominated case ( $\lambda_T = 0.09$ ) using different turbulence models with the experimental data of Coren. Note that  $z/s = 0$  corresponds to the rotor surface and  $z/s = 1$  to the stator surface. Figure 6 and 7 show a comparison of similar results for the throughflow dominated case ( $\lambda_T = 0.21$ ).

It can be seen from Figures 4 to 7 that there can be noticeable differences between the results obtained using the different turbulence models. The difference is more pronounced in the radial velocity distribution (Figures 4 and 6) and especially within the boundary layers. The results of the standard and realizable k- $\epsilon$  models are closer to the experimental data both for radial and tangential velocities. Results obtained using RSM (Reynolds

Stress Model) for tangential velocity show over-prediction of measured values. The same over-prediction also occurs in the computed value of the moment coefficient (see Table 1). While on average the RSM case requires about 50% more CPU time in comparison to the  $k$ - $\epsilon$  and  $k$ - $\omega$  models, obtaining a converged solution for it was challenging even with reduced values of the under-relaxation factors. Reaching convergence was also difficult for the RNG (Renormalisation group) model and it generally resulted in a more unstable solution compared to the other models. The maximum number of iterations for achieving the stabilised solution for the two  $k$ - $\epsilon$  (standard and realisable) and the two  $k$ - $\omega$  (standard and SST) models was about 2500. However, for the RNG model, the solution was not stabilised even after about 8,000 iterations. This could be due to the additional nonlinear terms in the governing equations of the RNG model. Compared with standard  $k$ - $\epsilon$  model, the additional terms in the  $\epsilon$ -equation of the RNG model augment  $\epsilon$ , reduce  $k$  and eventually the effective viscosity. This makes the RNG model to yield a lower turbulent viscosity in rapidly strained flows than the standard  $k$ - $\epsilon$  model. As a result, RNG model is subjected to instabilities in steady-state solutions in comparison with the standard  $k$ - $\epsilon$  model which is slightly over-diffusive and gives more stable solutions.

Tables 1 and 2 compare the computed values of moment coefficient with the experimental measurements for  $\lambda_T = 0.09$  and  $0.21$  respectively. The simulation results are generally in very good agreement with the experimental measurements. Furthermore it can be seen that the results of different turbulence models (with the exception of the RSM model) show only a small discrepancy from each other. As a result, it can be concluded that the moment coefficient has low sensitivity to the selection of turbulence model.

It is also worthwhile to comment on the effect of near wall treatments on the moment coefficient and velocity distributions. Using the enhanced wall treatment requires fine meshes near the walls, which increases the total number of points and, as a result, the CPU time for the simulation. Therefore, another mesh was generated for use with standard wall treatment. The effect of different near wall treatments on the velocity distribution across

the cavity at  $r/b = 0.79$  is shown in Figures 8, 9, 10 and 11. The radial and tangential velocities for  $\lambda_T = 0.09$  are shown in Figures 8 and 9 respectively and those for  $\lambda_T = 0.21$  in Figures 10 and 11 respectively. Two wall treatment schemes were used; standard wall function and enhanced wall treatment both with the  $k-\epsilon$  turbulence model. For  $\lambda_T = 0.21$  there is a generally good agreement between the two methods of wall treatment. Both schemes show separate boundary layer on the rotor and stator, separated by a core region where  $V_r = 0$  and  $V_t/\omega_r \approx 0.2$ . Radial outflow occurs in the rotor boundary layer and radial inflow in the stator boundary layer. This is consistent with a qualitative description of the flow provided by Batchelor (1951) (Figures 10 and 11), there are significant differences between the radial velocities obtained from the two methods. However, there is very little difference in the tangential velocity. For the value of  $\lambda_T = 0.21$ , the flow structure is expected to be dominated by the throughflow rate and it can be seen to be in broad agreement with Stewartson's (1952) description. There is a boundary layer adjacent to the rotor with both radial and tangential velocity gradients and almost a zero tangential velocity everywhere outside of this boundary layer. A positive radial velocity exists between rotor and stator adjacent to the rotor; this is augmented due to the pumping effect of the rotor. In contrast, near the stator there is little or no evidence of a boundary layer. It can be seen from Figure 10 that, the standard wall function approach fails to predict a negative radial velocity near the stator but the enhanced wall treatment gives results that are more consistent with the experimental data shown in Figure 6. This could be due to the modelling method of the near wall region for the standard wall function, in which the viscosity-affected region is not resolved and is bridged by the wall function directly to the turbulent core. It appears from Figure 10 that the negative radial velocity region near the stator is not predicted by the standard wall function. This results in an over-prediction of radial velocity in that region and since the radial velocity continues to increase away from the stator, this over-prediction will accordingly continue across the whole width of the cavity. For  $\lambda_T = 0.09$  (Figures 8 and 9) the disparity is less than for  $\lambda_T = 0.21$  and only occurs close to the stator ( $z/s \approx 1$ ).

Tables 3 and 4 show a comparison between the simulation results of moment coefficient for  $\lambda_T = 0.09$  and  $\lambda_T = 0.21$  respectively the two using different near wall treatments. It can be seen that the standard wall function gives a lower value of the moment coefficient (by about 8%) compared to the results from the enhanced wall treatment. This happens because the standard wall function does not model the details of the laminar sub-layer and the buffer layer regions, and hence fails to accurately predict the viscous losses in those areas. However, it is important to note that the number of points for the mesh using the enhanced wall treatment is approximately twice the number of points for standard wall function. This results in a threefold increase in CPU time required to reach convergence. Although not too significant for the above 2D computations, the increase in computational costs is expected to be more pronounced for the 3D simulations that include the bolts where finer grids are required around the bolt. In addition, it should be noted that when the bolts are modeled, the effect of the pressure difference around the bolts is the main mechanism for torque production. Typically, the pressure field is not very sensitive to the different types of wall treatment. Consequently, and in the interest of computational efficiency, the standard wall function was chosen as the near wall treatment for modeling the 3-D bolt windage data.

Based on the results gathered in this validation exercise, it would appear that the standard k- $\epsilon$  model offers the best combination of computational accuracy combined with simplicity of use. In addition, it was found that the moment coefficient and the tangential velocity distribution have a relatively low sensitivity to the selection of turbulence model. Since those parameters are the main outputs of the simulations, the use of more complex models like SST-k- $\omega$  or RSM will not provide significant advantages. As a result, the standard k- $\epsilon$  turbulence model was chosen for the 3-D simulations.

## 4 CFD SIMULATIONS OF ROTOR MOUNTED BOLTS

As mentioned in Section 2, the bolt windage rig has a double sided disc and the experiments were carried out by balancing the flow to both sides. Balancing the test (front) and balance (rear) sides of the cavity was achieved by matching the mass flow together with the inlet and outlet pressures. As well as reducing the net axial load on the rotor, this also ensures minimum leakage at the peripheral seals between the front and rear sides of the disc. Consequently, it is possible to simulate one side of the cavity in isolation to reduce the mesh size by 50%.

In order to confirm that very little leakage occurred in the experiment, a plain disc two-sided model was simulated under four different conditions ( $Re_\phi = 2.7 \times 10^6, 5.78 \times 10^6, 8.02 \times 10^6$  and  $11.7 \times 10^6$  with  $C_w = 0.3 \times 10^5$ , ( $0.063 < \lambda_T < 0.21$ ). Figure 12 show the simulated geometry of the two-sided cavity.

The total viscous moment coefficient of the disc can be divided into three sources: that from the front side of the disc, that from the rear side of the disc, and that from the peripheral seal. Figure 13 shows the contributions of these sources of moment coefficient to the total for the four different rotational Reynolds numbers simulated. It can be seen that the moment coefficient of the front and rear sides are almost the same. This is also shown in Figure 14 which gives the percentage contribution of each component to the total moment coefficient. It is relevant to note that the moment coefficient for the peripheral seal is generally around 10% of the total moment coefficient (or  $1/9^{\text{th}}$  of the value obtained from the two disc surfaces).

This fact is used in subsequent computations where just one side of the cavity is modeled. The peripheral seal is not modeled, but the contribution to the total moment coefficient shows little significant variation with  $Re_\phi$  and is not expected to vary with  $C_w$ . The experimentally measured values of the moment coefficient take account of the frictional toques experienced on both sides of the disc and the peripheral seal. So, computed values from a

one-sided model of the cavity can be compared with the experimental values by doubling the computed values of  $C_m$  and then adding 11% of this value to represent the contribution of the peripheral seal.

Figure 15 shows part of the mesh used in the 3-D computational model for the bolt windage test rig. The periodic boundaries of the sector modelled lie mid-way between the bolts. So for 3 bolts a  $120^\circ$  sector is used, for 9 bolts a  $40^\circ$  sector and for 18 bolts a  $20^\circ$  sector. There is an extended geometry at the outlet, and a pipe attached to the inlet. Unstructured grids were used in the  $r-\phi$  plane only. Finer grids are used near the bolt. The distances near the walls were specified to allow the use of the standard wall treatment. The number of points in the  $r-z$  plane is  $200 \times 30$ . The standard  $k-\epsilon$  model was used for simulations.

Two different flow conditions  $Re_\phi = 6.8 \times 10^6$ ,  $C_w = 10^5$  ( $\lambda_T = 0.35$ ) and  $Re_\phi = 7.2 \times 10^6$ ,  $C_w = 0.3 \times 10^5$  ( $\lambda_T = 0.09$ ) were used in this paper. The former corresponds to a throughflow dominated regime and the later a regime where rotational effects are expected to dominate. Other dimensional parameters are given in Table 5.

Figures 16 and 17 respectively show the variation of moment coefficient (on one side of the disc) with number of bolts  $N$  for:  $Re_\phi = 6.8 \times 10^6$ ,  $C_w = 10^5$  ( $\lambda_T = 0.35$ ) and  $Re_\phi = 7.2 \times 10^6$ ,  $C_w = 0.3 \times 10^5$  ( $\lambda_T = 0.09$ ). The experimental results, together with those from the CFD simulations are shown for  $N = 3, 9$  and  $18$  bolts as well as for a plain disc. The plain disc results are indicated by a continuous line for the experimental data and a dashed line for the CFD predictions. Both experimental data and CFD predictions show that, not surprisingly, the presence of bolts causes a significant rise in the moment coefficient above that of a plain disc and increasing  $N$  also increase  $C_m$ . Furthermore, it can be seen that the moment coefficient of the throughflow dominated case (Figure 16) is significantly higher than that of the rotationally dominated cases (Figure 17). The reason for this is that increasing throughflow brings about a decrease in the tangential velocity of the core region. This occurs due to conservation of angular momentum and is a well known phenomenon in a plain disc rotor-stator cavity (Owen and Rogers). However, as will be shown later in this paper, it is also true in a rotor-stator system with

rotor-mounted bolts. Consequently, the relative (rotor to core) tangential velocity is increased by an increase in superimposed flow and this leads to an increase in the moment coefficient due to an increase in skin friction. As can also be seen from the results shown in Figures 16 and 17, there is a good overall agreement between the predictions and experimental data and this gives confidence in the numerical model.

Further simulations were carried out for  $N = 36, 45, 52$  and  $60$  (for  $N = 60$ , the circumferential spacing between one bolt and the next is less than  $D/4$ ) and a continuous ring with 16 mm radial thickness and 11 mm height at  $r = 0.2$  m on the rotor. These results are summarised in Figures 18 and 19 for the two flow conditions, which again show the variation of moment coefficient with  $N$ . The CFD results shown in Figures 18 and 19 extend the range of those shown in the previous figures and provide a consistent picture of the effect of the number of bolts on the moment coefficient. There also appears to be a value of  $N$  for which  $C_m$  remains relatively unaffected by further increase in the number of bolts. For  $\lambda_T = 0.35$ , this occurs when  $N = 50$  and for  $\lambda_T = 0.09$  when  $N = 20$ . It is interesting to see from Figures 18 and 19 that the moment coefficient of the ring is approximately equal to the moment coefficient of a plain disc. This is in agreement with the investigations of Millward and Robinson (1989).

The effect of the number of bolts on the axial variation of dimensionless tangential velocity at  $r/b = 0.9$  is illustrated in Figures 20 and 21 for the two flow conditions investigated in Figures 16 to 19. The horizontal axis starts at  $z/s = 0.42$  which corresponds to the axial location of the top of the bolt or ring. The tangential velocity varies around the circumference of the bolt radius and the value used in these graphs is that obtained at the location of the centreline of the bolt.

It is clear from both Figures 20 and 21 that the presence of bolts on the rotor brings about an increase in the tangential velocity of the core ( $V_\phi/\omega_r$ ). Although increasing  $N$  generally increases  $V_\phi/\omega_r$ , there is a levelling off (as was noticed in the value of  $C_m$  referred to above). It is also interesting to note that although the plain disc ( $N$

= 0) values of  $V_\phi/\omega_r$  for  $\lambda_T = 0.35$  and  $\lambda_T = 0.09$  are quite different ( $V_\phi/\omega_r \approx 0.04$  and  $0.3$  respectively). This discrepancy reduces with the presence of bolts. In the limit of  $N = 60$ ,  $V_\phi/\omega_r \approx 0.8$  for both for  $\lambda_T = 0.35$  and  $\lambda_T = 0.09$ .

Similar trends occur when the turbulent flow in the wake behind the bolts is examined. This can be seen from Figures 22 and 23 which show contours of entropy in the region of the bolt radius at  $z/s = 0.02$  for the two flow conditions. The wake regions are known to have the highest values of entropy due to the rapid and irregular fluctuations of flow. It is apparent that the form of the wake changes with the number of bolts fitted to the rotor. Increasing the number of bolts (and decreasing the distance between the two neighbouring bolts) can lead to a situation where the wake of one bolt has not fully collapsed in advance of the following bolt. Comparing the shape of the wakes in Figures 22 and 23 it can be seen that decreasing the throughflow rate, causes the wakes to become more circumferential in its path around the bolt and for  $N \geq 18$  the wake falls on the upper section of the bolt. Although as explained previously in this paper, the skin friction is reduced as  $\lambda_T$  decreases. This does not account for the entire reduction in the overall moment coefficient. As can be seen in Figures 22 and 23, a decrease in  $\lambda_T$  also causes an increase of the wake shed from the trailing edge of one bolt with the leading edge of the next. This too brings about a reduction in  $C_m$  through the mechanism of form drag. There is also the (reversible) loss associated with the pumping mechanism of the bolts. It would be of interest to further investigate the contribution to  $C_m$ . However, since FLUENT reports only the viscous moment and pressure moment (which includes both the moment produced by the wakes and by pumping action) separately, it is not possible to find the amount of moment produced by the wakes alone.

Figures 24 and 25 show contours of relative total pressure at  $z/s = 0.02$  in the region of the bolt radius for  $N = 9, 18, 45,$  and  $60$  for the two flow conditions. Increasing the number of bolts, increases the peak total pressure but also decreases the relative total pressure difference across each individual bolt. This leads to a net decrease in

the moment due to a single bolt as a consequence of the increased influence of wakes from upstream bolts producing a smaller pressure difference across the bolt. However, since there are more bolts, the contribution of pressure-related moment of all bolts together increases.

The above results are summarised in Figures 26 and 27. This provides the contribution of skin friction and pressure-related (form drag and radial pumping) contributions to the overall moment coefficient for the two flow conditions. It is clear the skin friction contributes less to the overall moment coefficient than does pressure. As shown in Figures 26 and 27, the dominance of the pressure-related moment means that the net effect of increasing the number of bolts is to increase the overall moment coefficient. But for the reasons explained above concerning the structure of the wakes, the rate at which  $C_m$  increases with  $N$ , decreases as  $N$  becomes larger.

## **5 CONCLUSIONS**

This paper has presented CFD predictions of the flow in a rotor-stator cavity with a superimposed radial flow. The aim has been to investigate the effect on the moment coefficient and velocity distributions of varying the number of bolts on the rotor. This has been achieved by using a number of different 2D and 3D CFD models and the commercial code FLUENT.

A 2D CFD model was used for validation against experimental data and also to investigate the sensitivity of the CFD results to choice of turbulence model and wall treatment scheme. Although not the most accurate, a standard  $k-\epsilon$  turbulence model with a standard wall treatment was selected for the 3D computations as a compromise due to practical limitations in the CPU time. The test rig comprises a rotor in a pressurised casing

supplied with air. The outer radius of the rotor is  $b = 0.225$  m and the axial gap between the rotor and casing is 0.022 m.

Two (3D) test cases were used to examine the effects of rotor-mounted bolts: one corresponds to a regime where rotation will dominate the flow structure:  $Re_\phi = 7.2 \times 10^6$ ,  $C_w = 0.3 \times 10^5$  ( $\lambda_T = 0.09$ ) and the other where the flow is expected to be dominated by the superimposed radial flow  $Re_\phi = 6.8 \times 10^6$ ,  $C_w = 10^5$  ( $\lambda_T = 0.35$ ). Comparison is made with experimental data acquired at these conditions for  $N = 3, 9$  and 18 hexagonal bolts of 16 mm diameter and 11 mm height. The numerical study was extended to  $N = 0$  and  $18 < N \leq 60$  and also a continuous ring.

There is acceptable agreement between the values of moment coefficient obtained from the CFD predictions with the experimental data for these two test cases. There also appears to be very little difference between the values of  $C_m$  obtained for a plain disc with those for a continuous ring. Increasing the number of bolts creates an increase in the moment coefficient. However, this reaches a limit where further increases in  $N$  do not bring about an increase in  $C_m$ . This can be explained by examining the separate contributions that skin friction and pressure related drag make to the overall moment coefficient. The skin friction actually reduces as the number of bolts is increased. This is because increasing  $N$  causes the tangential velocity of the core to increase which decreases the relative rotor-to-core velocity. The pressure related drag (it was not possible to discriminate between form drag and pumping loss in this study) is also affected by increasing  $N$ . The more bolts fitted, the more the wake of the leading bolt affects that of the bolt immediately behind. As a result the drag for each bolt is reduced, but as there are more bolts, the overall drag increases. The direction of the wake shed by one bolt and therefore its influence on another bolt is also found to be affected by  $\lambda_T$ . A small value of  $\lambda_T$  will reduce the moment coefficient since the wake shed from one bolt becomes more circumferential and incident with the

leading edge of another. Conversely, a large value of  $\lambda_T$  causes the wake to become more radial since there is less shielding between one bolt and the next. As a result, the moment coefficient will increase with increasing  $\lambda_T$  and decrease with decreasing  $\lambda_T$ .

## **ACKNOWLEDGEMENTS**

The authors would like to thank Rolls-Royce PLC for funding the experimental work used for the validation of the CFD computations.

## **REFERENCES**

Batchelor, C. K. (1951) Note on a class of solutions to the Navier-Stokes Equations representing steady rotationally-symmetric flow. *Quart. J. Appl Math.* Vol 4, pp 29-41

Bayley, F.J., Owen, J.M., 1969, "Flow between a rotating and a stationary disc", *Aeronautical Quarterly*, Vol. 20, pp.333-354.

Coren, D., 2007. Windage due to Protrusions in Rotor-Stator Systems, D.Phil. thesis, Thermo-Fluid Mechanics Research Centre, University of Sussex, Brighton, UK.

Daily, J. W. and Nece, R. E. Chamber dimension effects on induced flow and frictional resistance of enclosed rotating discs. *J. Basic Eng.*, 1960, 82, 217–232.

Dibelius, G., Radtke, F., Ziemann, M., 1984. Experiments on Friction, Velocity and Pressure Distribution of Rotating Discs, *Heat and mass transfer in rotating machinery.* (A86-24451 09-34), Washington, DC, Hemisphere Publishing Corp., pp. 117-130.

Gartner, W. 1997 A Prediction Method for the Frictional Torque of a Rotating Disc in a Stationary Housing with a Superimposed Radial Outflow. ASME Gas Turbine and Aeroengine Congress and Exposition, Paper No. 97-GT-204.

Gartner, W., 1998. A Momentum Integral Method to Predict the Frictional Torque of a Rotating Disc with Protruding Bolts, ASME conference paper, 98-GT-138.

Millward, J.A., Robinson, P.H., 1989. Experimental Investigation into the Effects of Rotating and Static Bolts on Both Windage Heating and local Heat Transfer Coefficients in a Rotor-Stator Cavity, Gas turbine and aeroengine congress and exposition paper, 89-GT-196.

Owen, J. M., Rogers, R. H., 1989, "Flow and Heat Transfer in Rotating-Disc Systems." Volume one – Rotor-Stator Systems, Research Studies Press Ltd., ISBN 0 86380 090 4.

Stewartson, K., 1952, "On the flow between two rotating coaxial discs", Proc. Camb. Phil. Soc. Vol.49, pp. 333-341.

Von Kármán, T., 1921, "Technical Memorandum on Laminar and Turbulent Friction", National advisory committee for aeronautics, Report No. 1092.

Zimmerman, H., Firsching, A., Dibelius, G.H., Ziemann, M., 1986. Friction Losses and Flow Distribution for Rotating Discs with Shielded and Protruding Bolts, ASME conference paper, 86-GT-158.

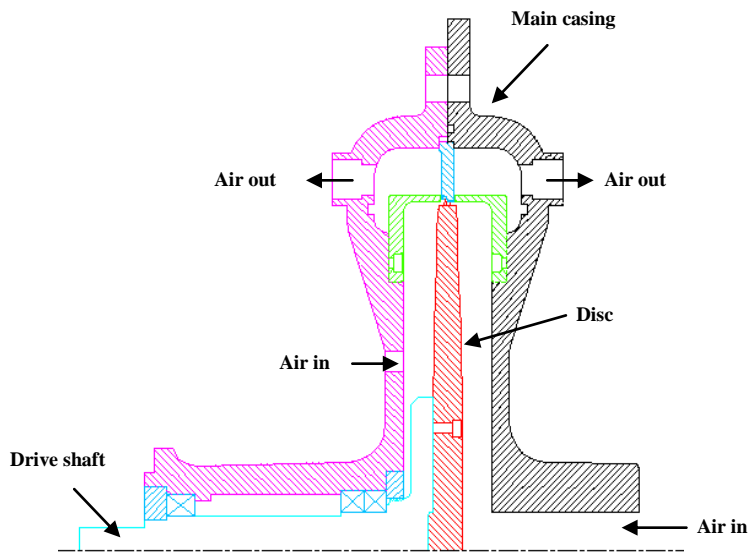
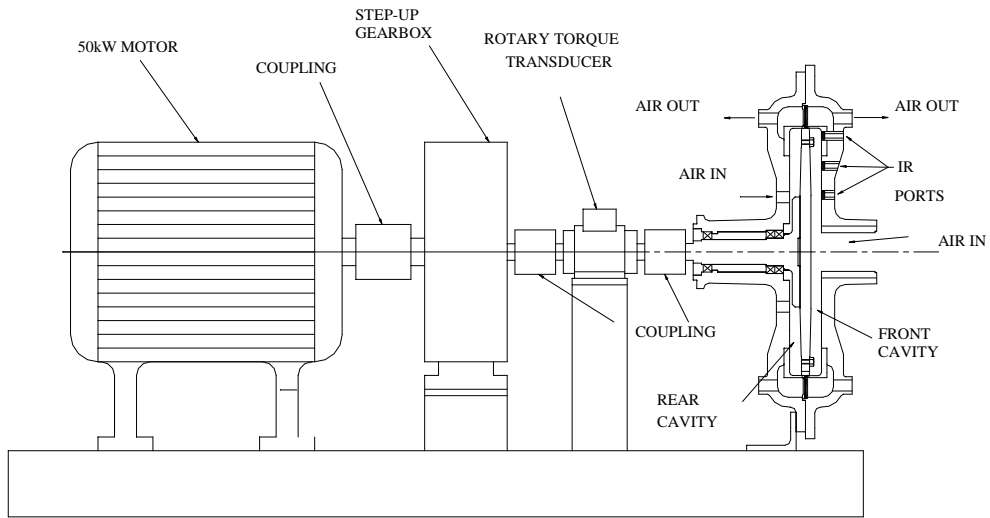


Figure 1: Schematic Diagram of the Bolt Windage Test Rig

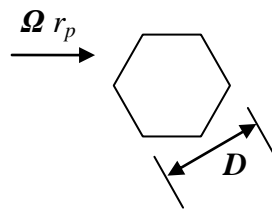


Figure 2: Orientation of Bolts with Respect to Rotation.

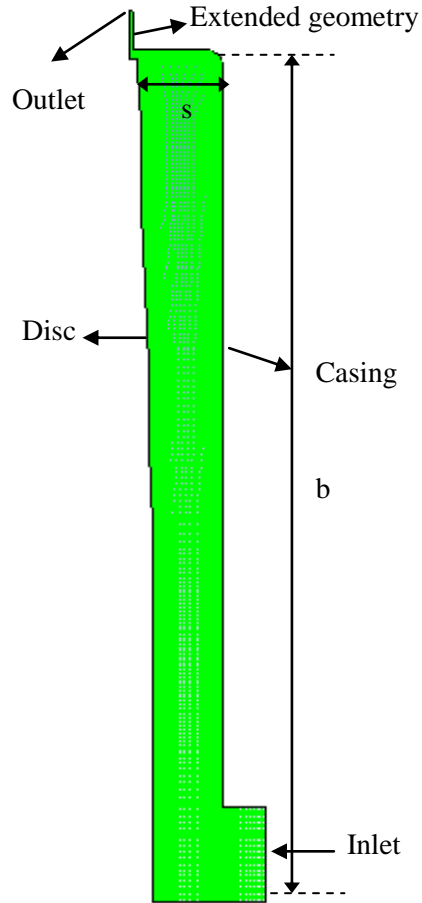


Figure 3: Schematic diagram of the 2D simulated geometry

Figure 4: Comparison between the Axial Distribution of Dimensionless Radial Velocity for Different Turbulence Models with the Experimental Data of Coren (2007) at  $r/b = 0.79$ ,  $\lambda_T = 0.09$ ,  $C_w = 0.3 \times 10^5$   
 Note:  $z/s = 0$  is located on the rotor. This is also the case for Figures 5 to 11.

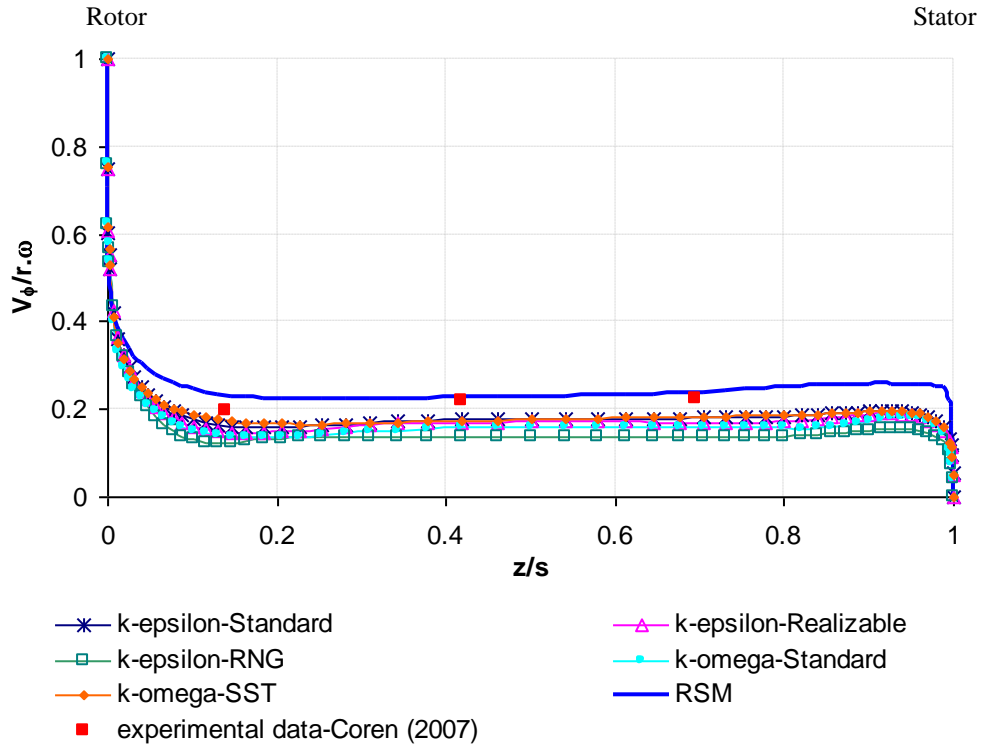


Figure 5: Comparison between Axial Distribution of Dimensionless Tangential Velocity for Different Turbulence Models with the Experimental Data of Coren (2007) at  $r/b = 0.79$ ,  $\lambda_T = 0.09$ ,  $C_w = 0.3 \times 10^5$

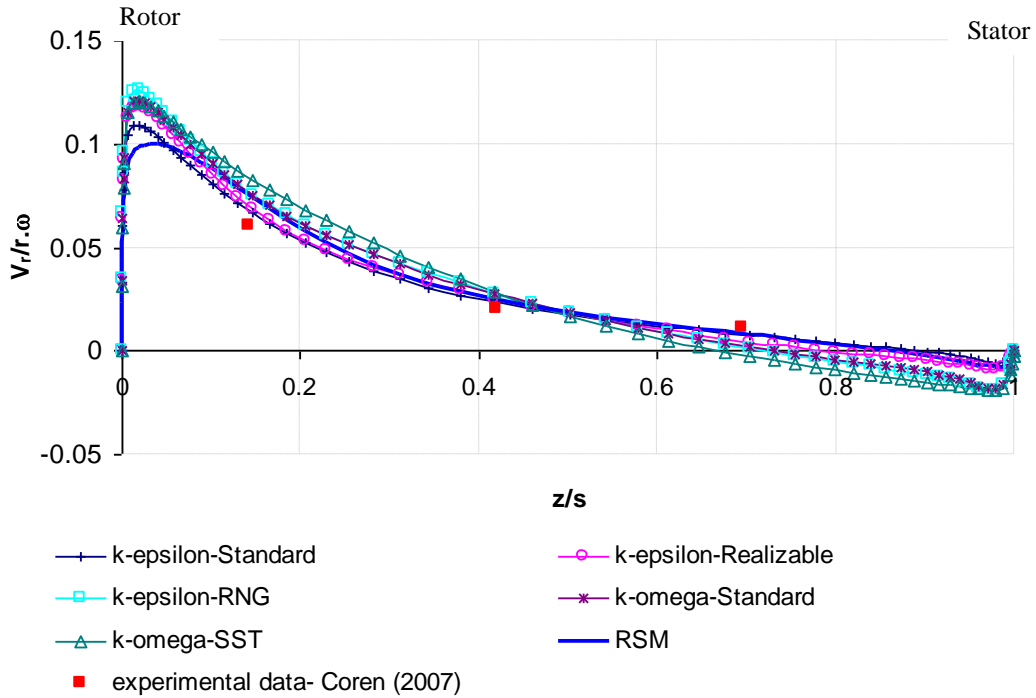
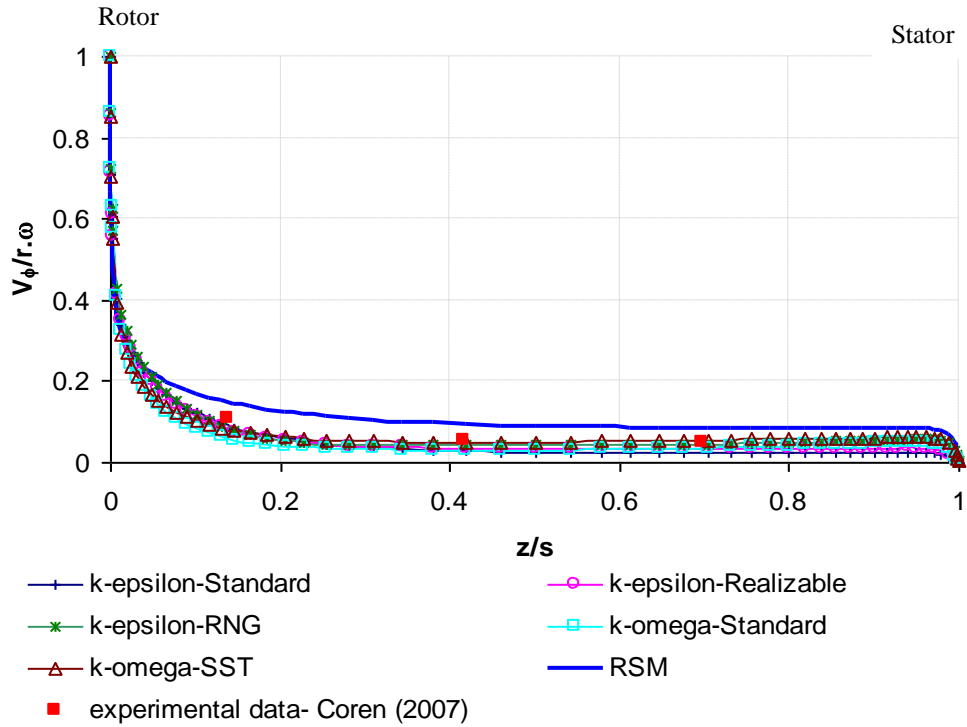
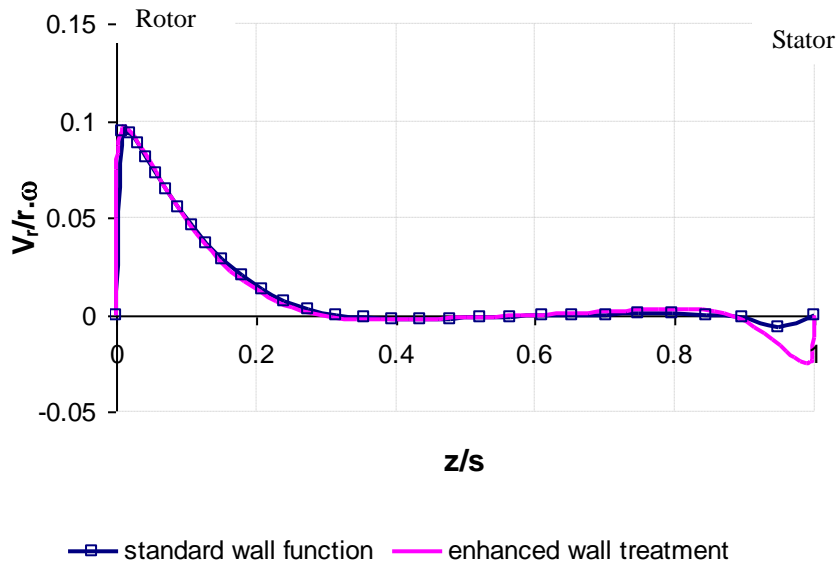


Figure 6: Comparison between the Axial Distribution of Dimensionless Radial Velocity for Different Turbulence Models with the Experimental Data of Coren (2007) at  $r/b = 0.79$ ,  $\lambda_T = 0.21$ ,  $C_w = 0.3 \times 10^5$



**Figure 7: Comparison between the Axial distribution of Dimensionless Tangential Velocity for Different Turbulence Models with the Experimental Data of Coren (2007) at  $r/b = 0.79$ ,  $\lambda_T = 0.21$ ,  $C_w = 0.3 \times 10^5$**



**Figure 8: Simulation Results of Radial Velocity at  $r/b = 0.79$  for Different near Wall Treatments, Using the Standard k- $\epsilon$  Model,  $\lambda_T = 0.09$ ,  $C_w = 0.3 \times 10^5$**

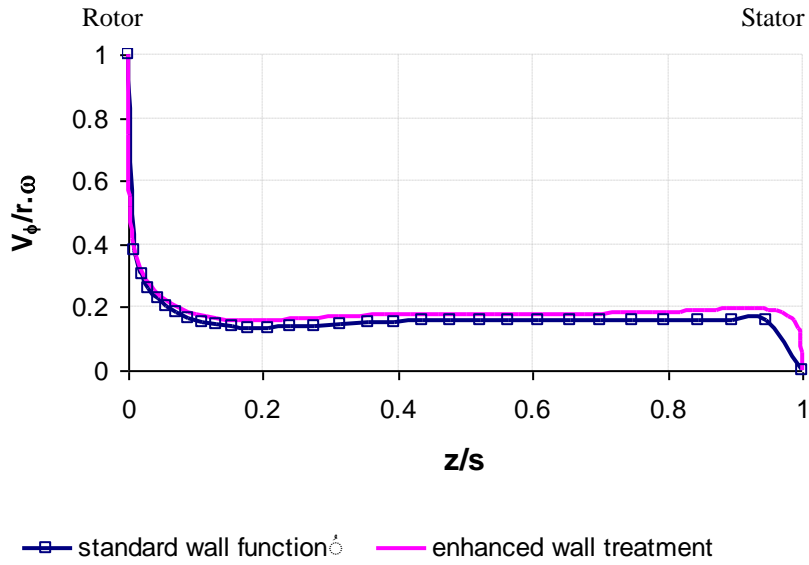


**Figure 9: Simulation Results of Tangential Velocity at  $r/b = 0.79$  for Different near Wall Treatments, Using the Standard  $k-\epsilon$  Model,  $\lambda_T = 0.09$ ,  $C_w = 0.3 \times 10^5$**

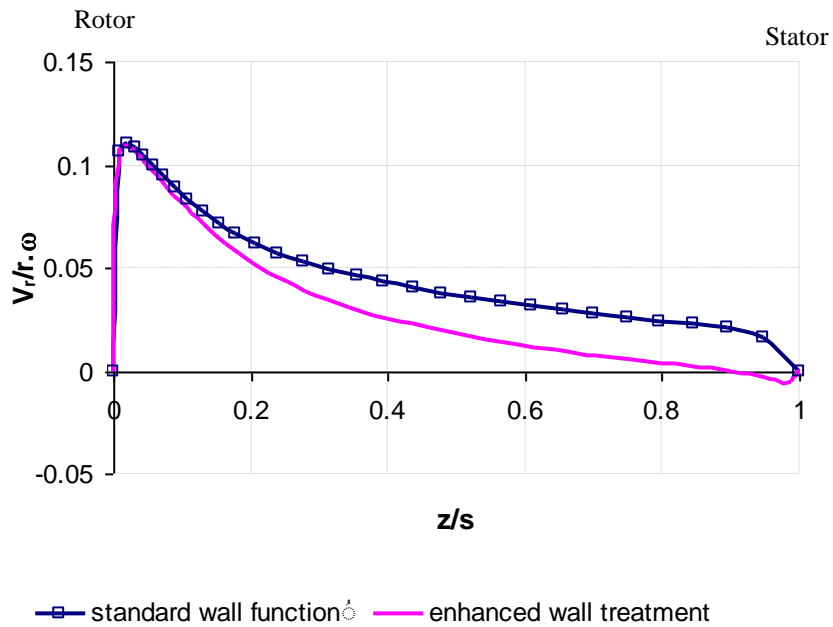


**Figure 10: Simulation Results of Radial Velocity at  $r/b = 0.79$  for Different near Wall Treatments, Using the Standard  $k-\epsilon$  Model,  $\lambda_T = 0.21$ ,  $C_w = 0.3 \times 10^5$**

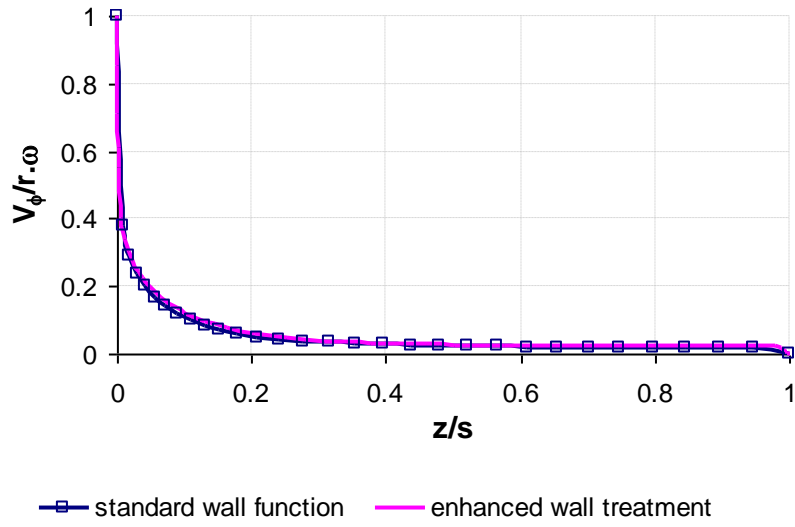


**Figure 11: Simulation Results of Tangential Velocity at  $r/b = 0.79$  for Different near Wall Treatments, Using the Standard  $k-\epsilon$  Model,  $\lambda_T = 0.21$ ,  $C_w = 0.3 \times 10^5$**

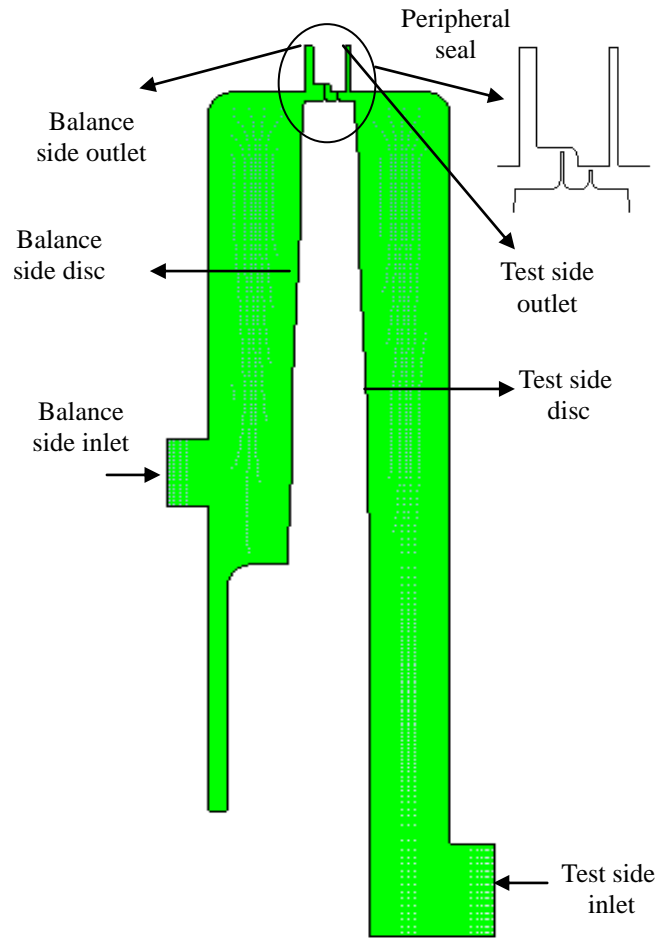


**Figure 12: Schematic diagram of the two-sided simulated geometry**

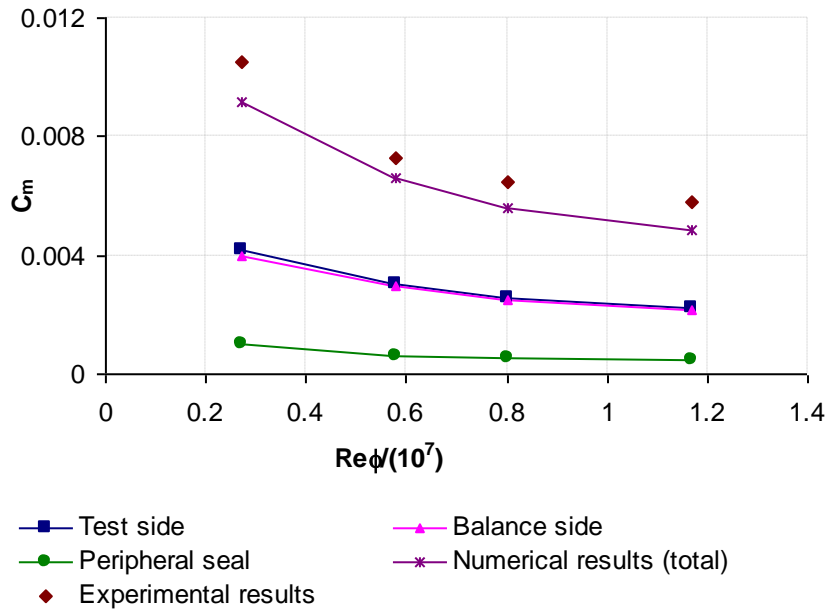


Figure 13: Contribution to the total moment coefficient produced by the different rotating components in the simulated two sided plain disc geometry,  $C_w = 0.3 \times 10^5$

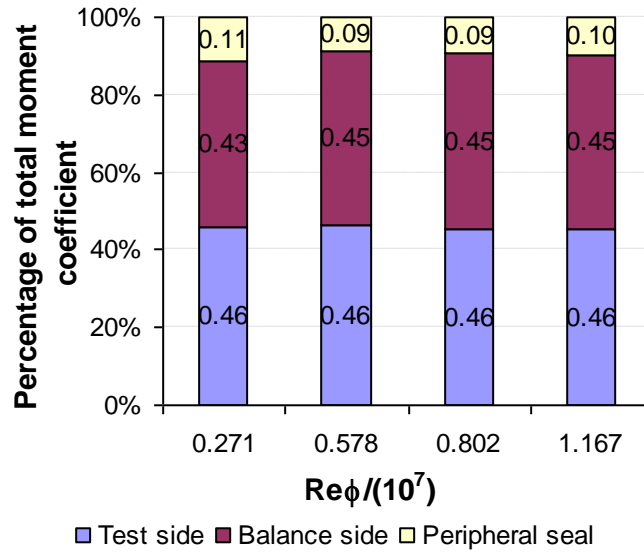


Figure 14: Contribution of the different rotating components in the simulated two-sided plain disc geometry,  $C_w = 0.3 \times 10^5$

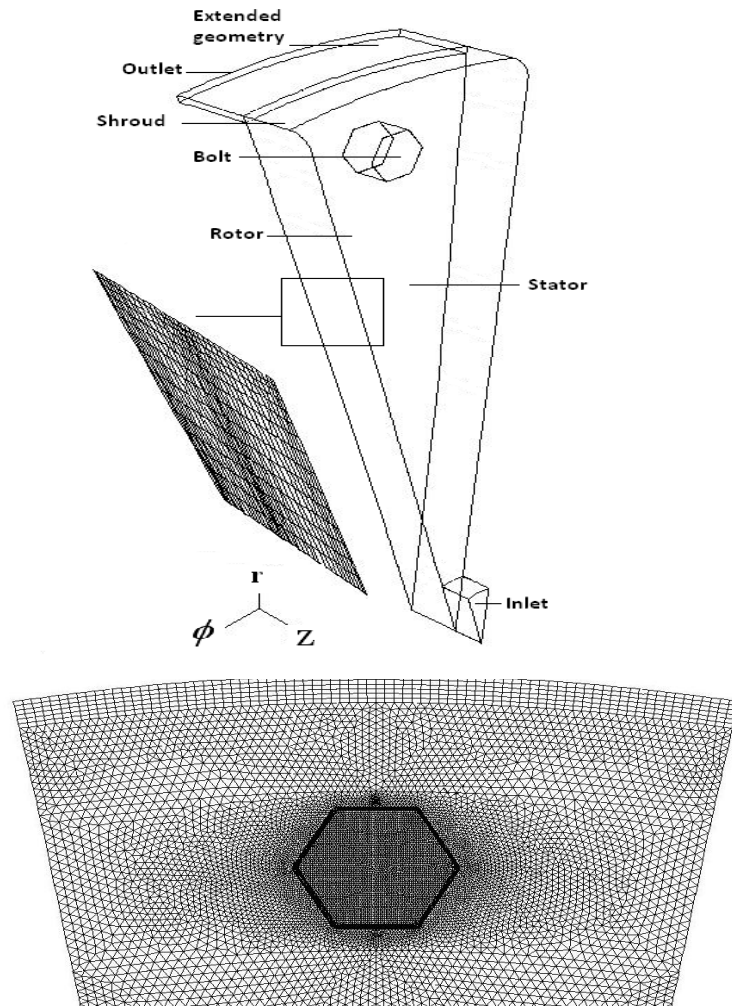


Figure 15: A Section of the Computational Mesh used for the Bolt Windage Test Rig

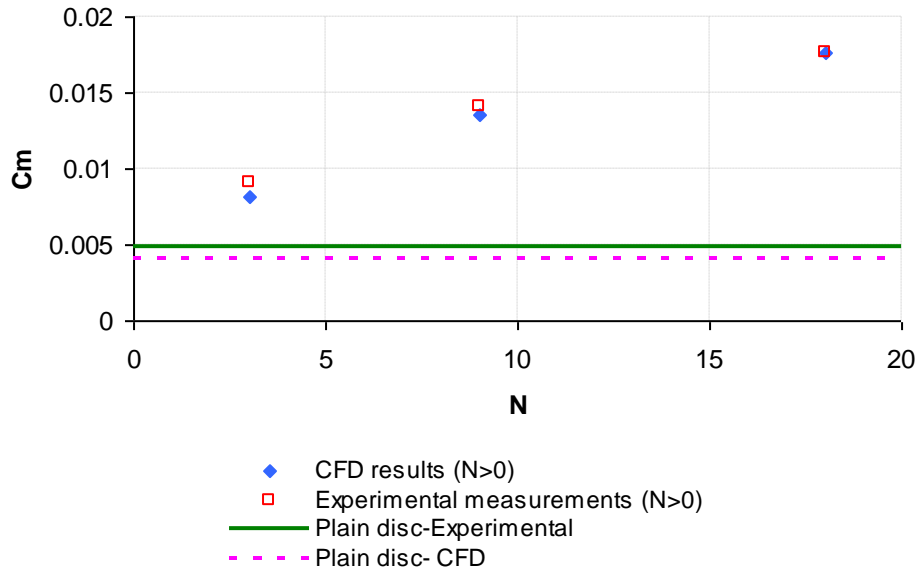


Figure 16: Variation of Moment Coefficient with Number of Bolts N. Comparison Between Numerical and Experimental Results for 3, 9 and 18 bolts and also a plain disc:  $Re_\phi = 6.8 \times 10^6$ ,  $C_w = 10^5$  ( $\lambda_T = 0.35$ )

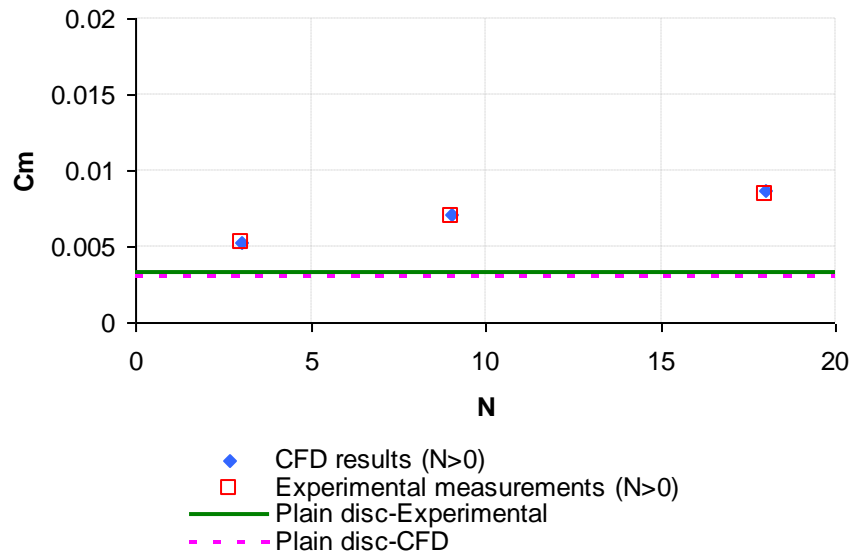


Figure 17: Variation of Moment Coefficient with Number of Bolts N. Comparison Between Numerical and Experimental Results for 3, 9 and 18 bolts and also a plain disc:  $Re_\phi = 7.2 \times 10^6$ ,  $C_w = 0.3 \times 10^5$  ( $\lambda_T = 0.09$ )

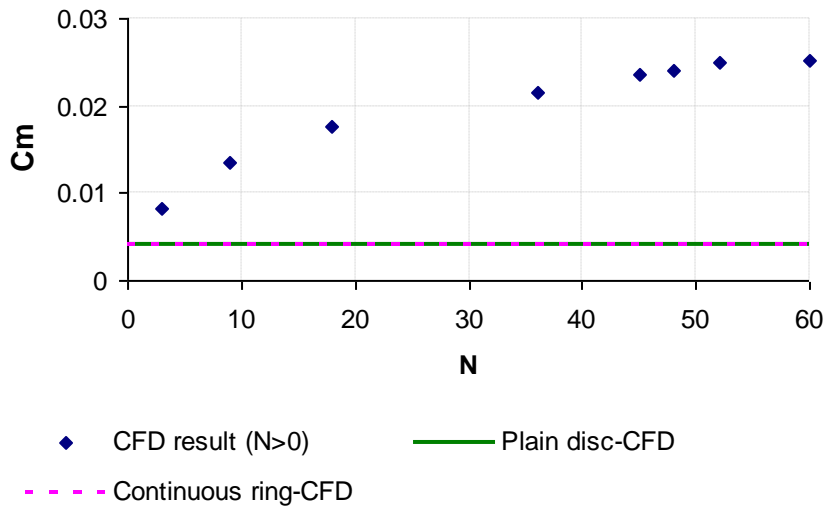


Figure 18: Predicted Variation of Moment Coefficient with Number of Bolts, N for  $Re_\phi = 6.8 \times 10^6$ ,  $C_w = 10^5$  ( $\lambda_T = 0.35$ ).

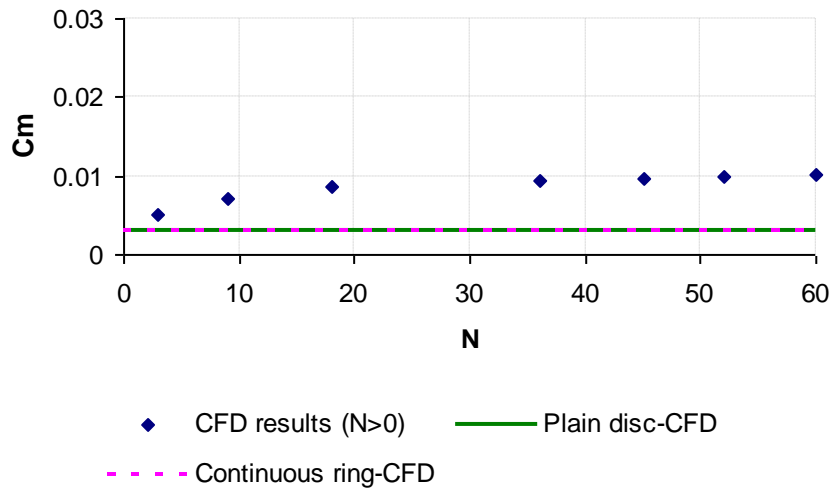


Figure 19: Predicted Variation of Moment Coefficient with Number of Bolts, N for  $Re_\phi = 7.2 \times 10^6$ ,  $C_w = 0.3 \times 10^5$  ( $\lambda_T = 0.09$ ).

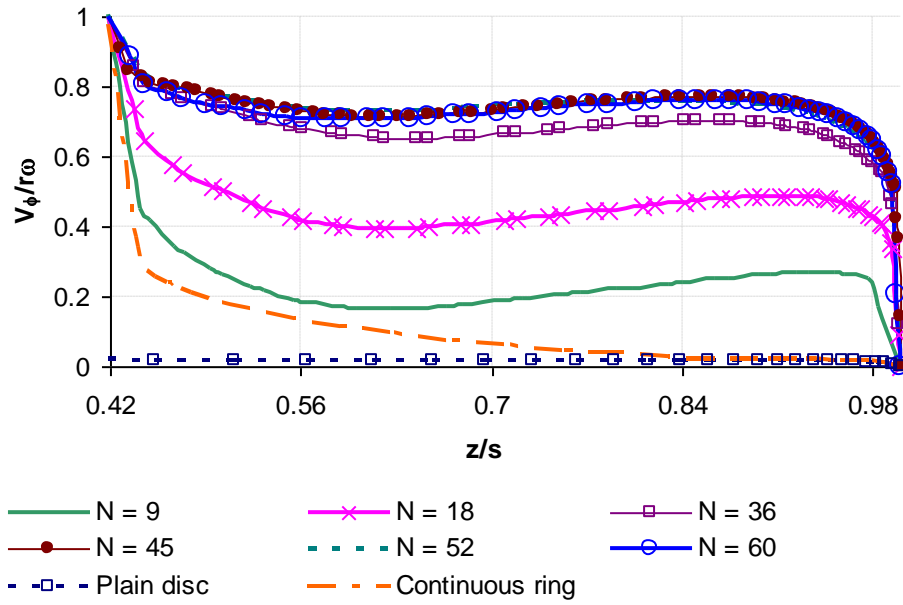


Figure 20: Predicted Axial Variation of Dimensionless Tangential Velocity at  $r/b = 0.9$ ,  $Re_\phi = 6.8 \times 10^6$  and  $C_w = 10^5$  ( $\lambda_T = 0.35$ ). Note:  $z/s = 0$  is located on rotor. This is also the case for Figure 21.

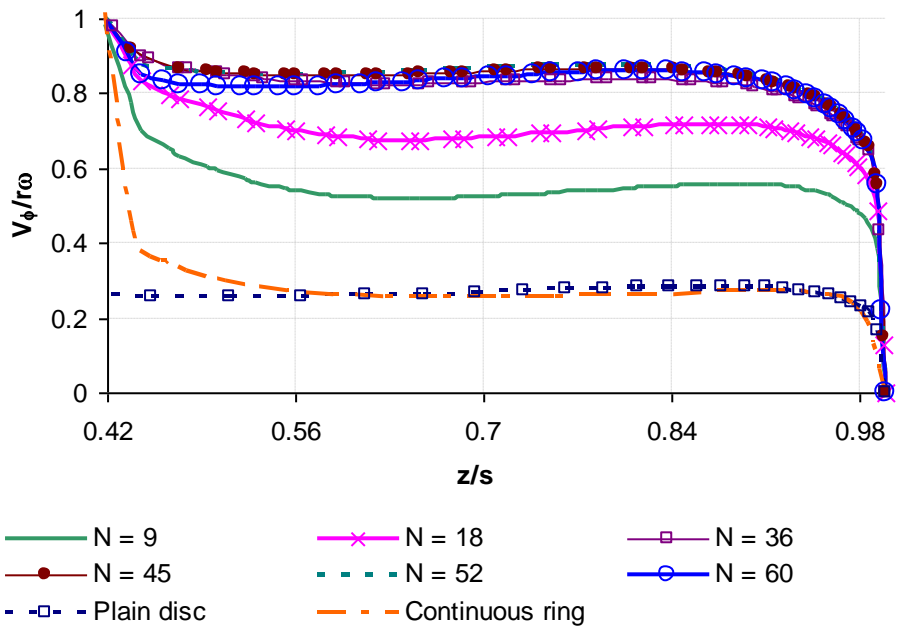


Figure 21: Predicted Axial Variation of Dimensionless Tangential Velocity at  $r/b = 0.9$ ,  $Re_\phi = 7.2 \times 10^6$  and  $C_w = 0.3 \times 10^5$  ( $\lambda_T = 0.09$ ).

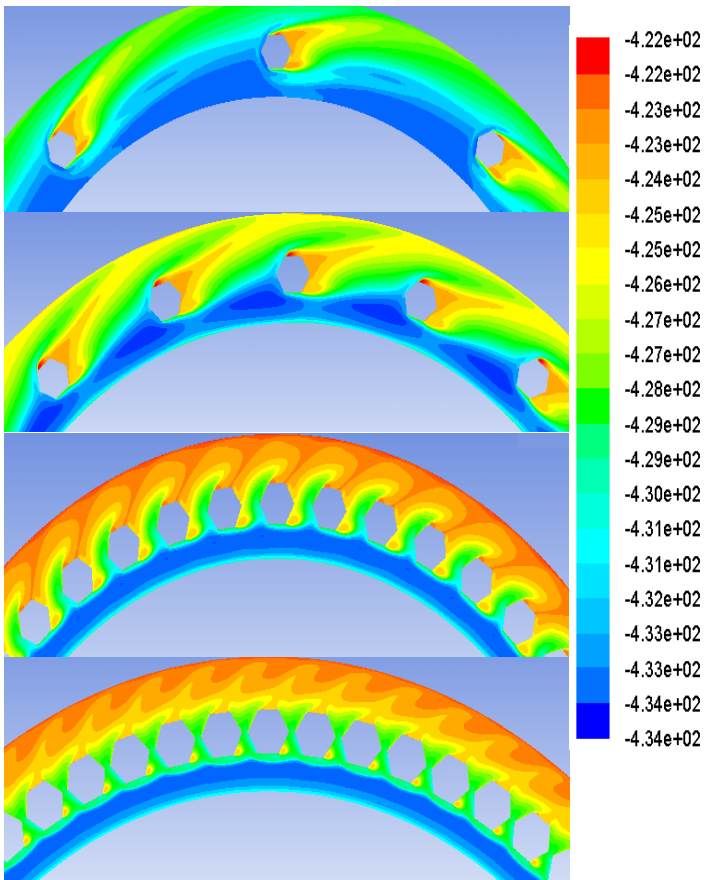


Figure 22: Entropy Contours around the Bolts for  $N = 9, 18, 45$  and  $60$  ( $Re_\phi = 6.8 \times 10^6$ ,  $C_w = 10^5$  and  $\lambda_T=0.35$ ) at  $z/s = 0.02$

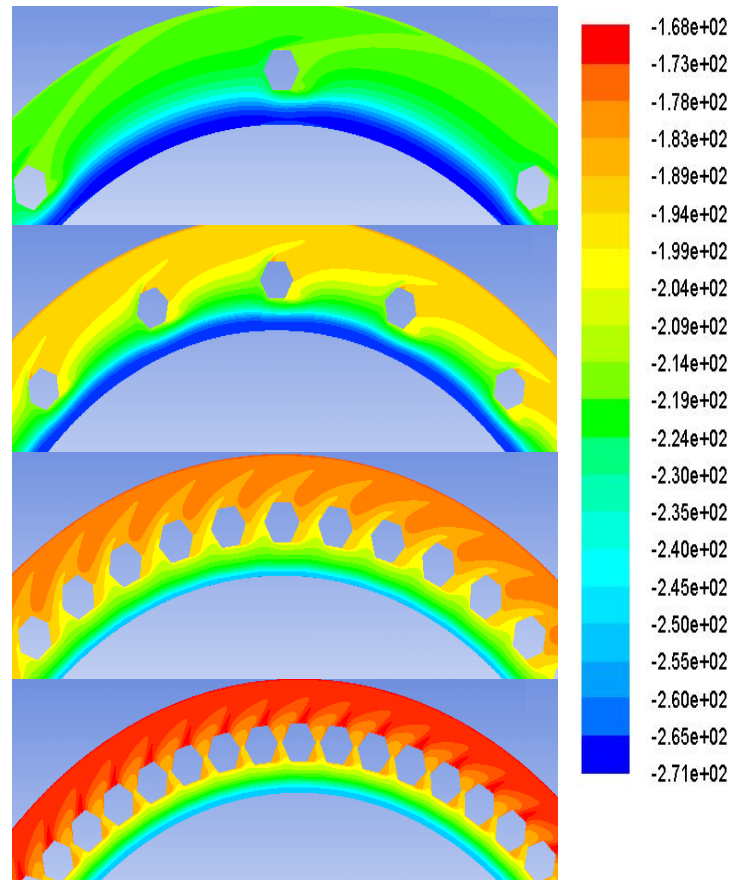


Figure 23: Entropy Contours around the Bolts for  $N = 9, 18, 45$  and  $60$  ( $Re_\phi = 7.2 \times 10^6$ ,  $C_w = 0.3 \times 10^5$  and  $\lambda_T=0.09$ ) at  $z/s = 0.02$

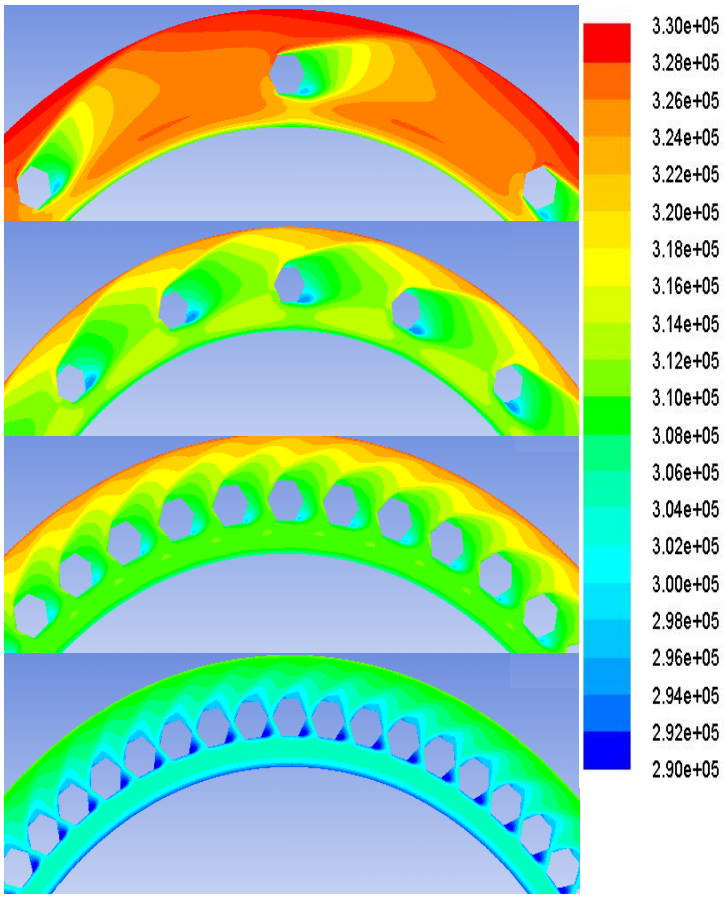


Figure 24: Relative total pressure Contours around the Bolts for  $N = 9, 18, 45$  and  $60$  ( $Re_\phi = 6.8 \times 10^6$ ,  $C_w = 10^5$  and  $\lambda_T = 0.35$ ) at  $z/s = 0.02$

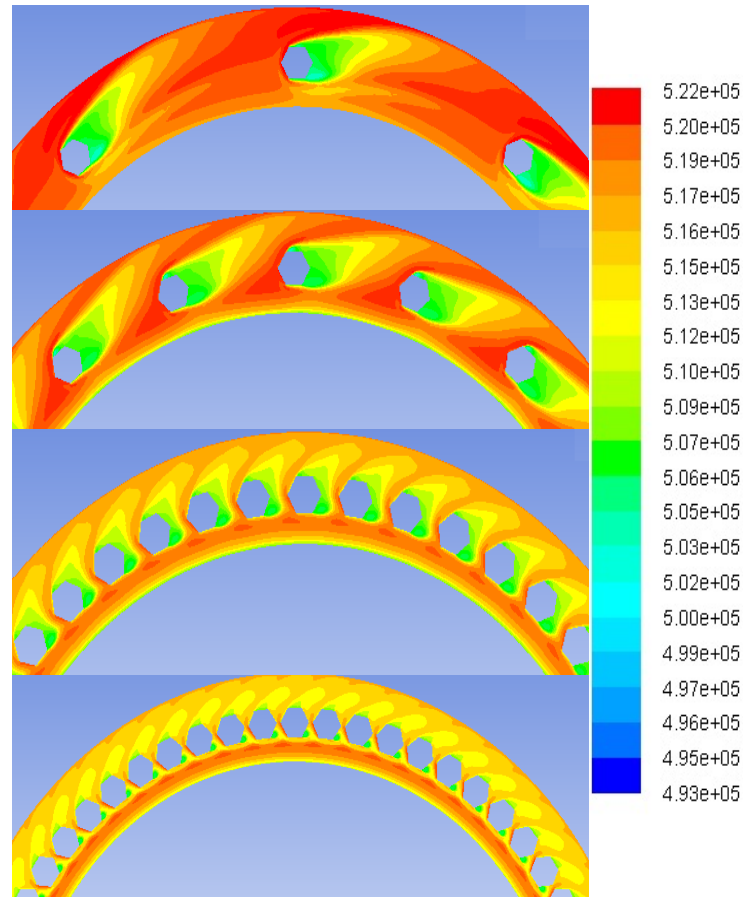


Figure 25: Relative total pressure Contours around the Bolts for  $N = 9, 18, 45$  and  $60$  ( $Re_\phi = 7.2 \times 10^6$ ,  $C_w = 0.3 \times 10^5$  and  $\lambda_T = 0.09$ ) at  $z/s = 0.02$

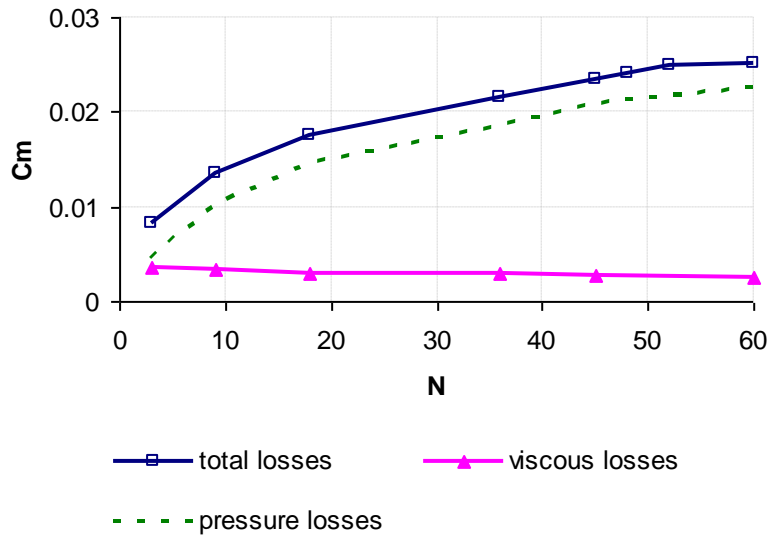


Figure 26: Variation of the overall moment coefficient, viscous and pressure-related (form drag and radial pumping) contributions with number of bolts ( $Re_{\phi} = 6.8 \times 10^6$  and  $C_w = 10^5$  and  $\lambda_T=0.35$ ).

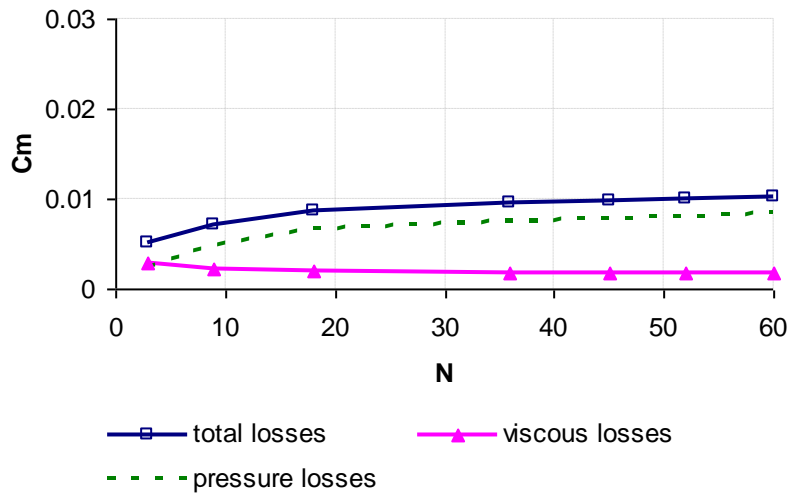


Figure 27: Variation of the overall moment coefficient, viscous and pressure-related (form drag and radial pumping) contributions with number of bolts ( $Re_{\phi} = 7.2 \times 10^6$ ,  $C_w = 0.3 \times 10^5$  and  $\lambda_T=0.09$ ).

**Table 1: Comparison of the Moment Coefficient Results of Different Turbulence Models with the Experimental Data of Coren (2007),  $\lambda_T = 0.09$ ,  $C_w = 0.3 \times 10^5$**

Model	$C_m$ (two sides)
$k - \varepsilon$ - Standard	0.00686
$k - \varepsilon$ - Realizable	0.00676
$k - \varepsilon$ -RNG	0.00647
$k - \omega$ - Standard	0.0063
$k - \omega$ - SST	0.0066
RSM	0.0095
Experimental data- Coren (2007)	0.0068

**Table 2: Comparison of the Moment Coefficient Results of Different Turbulence Models with the Experimental Data of Coren (2007),  $\lambda_T = 0.21$ ,  $C_w = 0.3 \times 10^5$**

Model	$C_m$ (two sides)
$k - \varepsilon$ - Standard	0.009905
$k - \varepsilon$ - Realizable	0.00979
$k - \varepsilon$ - RNG	0.00929
$k - \omega$ - Standard	0.0089
$k - \omega$ - SST	0.00932
RSM	0.013
Experimental data- Coren (2007)	0.0105

**Table 3: Comparison of Moment Coefficient for Different near Wall Treatments, Using the Standard  $k-\varepsilon$  Model,  $\lambda_T = 0.09$ ,  $C_w = 0.3 \times 10^5$**

Model	$C_m$ (two sides)
Standard $k - \varepsilon$ , Enhanced wall treatment	0.00686
Standard $k - \varepsilon$ , Standard wall function	0.00635
Experimental data, Coren (2007)	0.0068

**Table 4: Comparison of Moment Coefficient for Different near Wall Treatments, Using the Standard k- $\varepsilon$  Model,  $\lambda_T = 0.21$ ,  $C_w = 0.3 \times 10^5$**

<b>Model</b>	<b>Cm (two sides)</b>
Standard $k - \varepsilon$ , Enhanced wall treatment	0.009905
Standard $k - \varepsilon$ , Standard wall function	0.009
Experimental data, Coren (2007)	0.0105

**Table 5: Simulated flow conditions of the Bolt Windage Rig 3D case**

	<b>Flow condition 1</b>	<b>Flow condition 2</b>
$\dot{m}$ (kg/s)	0.415	0.119
$Re_\phi$	$6.8 \times 10^6$	$7.2 \times 10^6$
$C_w$	$10^5$	$0.3 \times 10^5$
$\lambda_T$	0.35	0.09
$\omega$ (rad/s)	409.5	902.5
$P_{inlet}$ (bar)	5.1	3
$T_{inlet}$ (K)	297	292



Dear sir/Madam

Could you please consider this paper for publication in your Journal. It is primarily the research work of a PhD student which builds on long term experimental research programme at the University of Sussex ThermoFluid Mechanics Research Centre.

Best regards

Abdulnaser Sayma